Nanoscale Research Letters
a SpringerOpen Journal

NANO EXPRESS   **Open Access**

Study on the visible-light-induced photokilling effect of nitrogen-doped TiO$_2$ nanoparticles on cancer cells

Zheng Li[1], Lan Mi[1*], Pei-Nan Wang[1] and Ji-Yao Chen[2]

Abstract

Nitrogen-doped TiO$_2$ (N-TiO$_2$) nanoparticles were prepared by calcining the anatase TiO$_2$ nanoparticles under ammonia atmosphere. The N-TiO$_2$ showed higher absorbance in the visible region than the pure TiO$_2$. The cytotoxicity and visible-light-induced phototoxicity of the pure- and N-TiO$_2$ were examined for three types of cancer cell lines. No significant cytotoxicity was detected. However, the visible-light-induced photokilling effects on cells were observed. The survival fraction of the cells decreased with the increased incubation concentration of the nanoparticles. The cancer cells incubated with N-TiO$_2$ were killed more effectively than that with the pure TiO$_2$. The reactive oxygen species was found to play an important role on the photokilling effect for cells. Furthermore, the intracellular distributions of N-TiO$_2$ nanoparticles were examined by laser scanning confocal microscopy. The co-localization of N-TiO$_2$ nanoparticles with nuclei or Golgi complexes was observed. The aberrant nuclear morphologies such as micronuclei were detected after the N-TiO$_2$-treated cells were irradiated by the visible light.

Introduction

Semiconductor titanium dioxide (TiO$_2$) has been widely studied as a photocatalyst for its high chemical stability, excellent oxidation capability, good photocatalytic activity, and low toxicity [1-4]. Under the irradiation of ultraviolet (UV) light with the wavelength shorter than 387 nm (corresponding to 3.2 eV for the band gap of anatase TiO$_2$), the electrons in the valence band of TiO$_2$ can be excited to the conduction band, thus creating the pairs of photo-induced electron and hole. Then, the photo-induced electrons and holes can lead to the formation of various reactive oxygen species (ROS), which could kill bacteria, viruses, and cancer cells [5-10].

In recent years, TiO$_2$ attracted more attention as a photosensitizer in the field of photodynamic therapy (PDT) due to its low toxicity and high photostability [2,3]. However, TiO$_2$ can be activated by UV light only, which hinders its applications. Improvement of the optical absorption of TiO$_2$ in the visible region by dye-adsorbed [11,12] or doping [13,14] methods will facilitate the practical application of TiO$_2$ as a photosensitizer for PDT. When using dye-adsorbed method, the dyes such as hypocrellin B [11] and chlorine e6 [12] themselves are well-known PDT sensitizers and will have influence on the PDT efficiency of TiO$_2$. For doping method, anionic species are preferred for the doping rather than cationic metals which have a thermal instability and an increase of the recombination centers of carriers [14]. In addition, cationic metals themselves always present cytotoxicity. Therefore, anionic species doping, especially nitrogen doping, is mostly adopted to improve the absorption of TiO$_2$ in the visible region.

In the present work, the nitrogen-doped TiO$_2$ (N-TiO$_2$) nanoparticles were used as the photosensitizer to test its photokilling efficiency for three types of cancer cell lines. The N-TiO$_2$ nanoparticles were prepared by calcining pure anatase TiO$_2$ nanoparticles under ammonia atmosphere, which was an inexpensive method and easy to operate. The produced N-TiO$_2$ nanoparticles have high stability and effective photocatalytic activity. Their absorption in the visible region was improved and their photokilling efficiency of cells under visible-light irradiation was compared with that of the pure TiO$_2$. The intracellular distributions of these nanoparticles were measured by the laser scanning confocal

* Correspondence: lanmi@fudan.edu.cn
[1]Key Laboratory of Micro and Nano Photonic Structures (Ministry of Education), Department of Optical Science and Engineering, Fudan University, Shanghai 200433, China
Full list of author information is available at the end of the article

SpringerOpen

microscopy (LSCM). The mechanisms of the photokilling effect were discussed.

Methods

Preparation and characterization of N-TiO$_2$ nanoparticles

The anatase TiO$_2$ nanoparticles (Sigma-Aldrich, St. Louis, MO, USA; particle size <25 nm) were calcined under ammonia atmosphere with various calcination parameters, such as temperature, gas flow rate, and calcination time, and then cooled down in nitrogen flow to the room temperature. Three N-TiO$_2$ samples prepared with different calcination parameters were used in this work. Together with the pure TiO$_2$, they are denoted as listed in Table 1. The crystalline phases of these samples were determined by Raman spectra (LABRAM-1B; HORIBA, Jobin Yvon, Kyoto, Japan). To evaluate their absorptions in the visible region, the ultraviolet-visible (UV/Vis) diffuse reflectance absorption spectra of these samples were measured with a Jasco V550 UV/Vis spectrophotometer (Jasco, Inc., Tokyo, Japan)

Pure- and N-TiO$_2$ nanoparticles were dispersed in Dulbecco's modified Eagle's medium with high glucose (DMEM-H), respectively, at various concentrations between 50 and 200 μg/mL. To avoid aggregation, these suspensions were ultrasonically processed for 15 min before using.

Cell culture

The human cervical carcinoma cells (HeLa), human hepatocellular carcinoma cells (QGY), or human nasopharyngeal carcinoma cells (KB) procured from the Cell Bank of Shanghai Science Academy (Shanghai, China) were grown in 96-well plates or Petri dishes in DMEM-H solution supplemented with 10% fetal calf serum in a fully humidified incubator at 37°C with 5% CO$_2$ for 24 h. Then, the culture medium was replaced by TiO$_2$-containing medium and the cells were incubated for 2 h in the dark. After the TiO$_2$ nanoparticles deposited and adhered to the cells, the medium was changed to the TiO$_2$-free DMEM-H solution supplemented with 10% fetal calf serum for further study.

Measurements of photokilling effect and cytotoxicity

To examine the photokilling effect, the cells were irradiated with the visible light from a 150-W Xe lamp (Shanghai Aojia Electronics Co. Ltd., Shanghai, China). Two pieces of quartz lens were used to obtain a concentrated parallel light beam. An IR cutoff filter was set in the light path to avoid the hyperthermia effect. A 400-nm longpass filter was used to cut off the UV light. The visible-light power density at the liquid surface in cell wells was 12 mW/cm^2 as measured by a power meter (PM10V1; Coherent, Santa Clara, CA, USA). After irradiation with this visible light for 4 h, cells were incubated in the dark for another 24 h until further analysis were conducted. The cytotoxicity examinations were carried out with the same procedure as the photokilling effect examinations but without the light irradiation, i.e., the TiO$_2$-treated cells were incubated in the dark for 28 h.

The cell viability assays were conducted by a modified MTT method using WST-8 [2-(2-methoxy-4-nitrophenyl)-3-(4-nitrophenyl)-5-(2,4-disulfophenyl)-2*H* tetrazolium, monosodium salt] (Beyotime, Jiangsu, China). Each well containing 100 μL culture medium was added with 10 μL of the WST-8 reagent solution, and the cells were then incubated at 37°C with 5% CO$_2$ for 2 h. Subsequently, the absorbance was measured at 450 nm using a microplate reader (Bio-Tek Synergy™ HT; Bio-Tek® Instruments, Inc., Winooski, VT, USA). The untreated cells were used as the control groups. The surviving fraction represents the ratio of the viable TiO$_2$-treated cells relative to that of the control groups. It should be noted that the TiO$_2$-containing DMEM-H solution will affect the absorbance value at 450 nm. Therefore, when measuring the cell viability, the absorbance values were measured as a reference before the WST-8 dyes were added. Each experiment was performed in triplicate and repeated three times.

Confocal laser scanning microscopy

The cells grown in Petri dishes were incubated with 50 μg/mL TiO$_2$ in DMEM-H for 10 h before the LSCM observation (Olympus, FV-300, IX71; Olympus, Tokyo, Japan). Hoechst 33342 (Beyotime) and BODIPY FL C$_5$-ceramide complexed to BSA (Molecular Probes; Invitrogen Corporation, Eugene, OR, USA) were used as the indicators for nucleus and Golgi complex, respectively. Hoechst 33342 (0.5 μg/mL) or Golgi complex marker (5 μM) was added into the growth medium for 15 to 30 min to stain the nuclei or Golgi complexes, respectively.

Table 1 Calcination parameters and the resulted crystalline phases of the TiO$_2$ nanoparticles

| Samples | Calcination parameters | | | Crystalline phases |
	Temperature (°C)	Ammonia gas flow rate (L/min)	Time (min)	
Pure	-	-	-	Anatase
N-550-1	550	3.5	20	Anatase
N-550-2	550	7	10	Anatase
N-600-1	600	3.5	20	Rutile and anatase

The reflection images of the intracellular TiO_2 nanoparticles and the fluorescence images of nuclei (or Golgi complexes) were simultaneously obtained by the LSCM in two channels with no filter for the reflecting light and a 585 to 640-nm bandpass filter for the fluorescence. A 488-nm continuous-wave (CW) Ar^+ laser (Melles Griot, Carlsbad, CA, USA) or a 405-nm CW semiconductor laser (Coherent) was used as the excitation source. A 60 × water objective was used to focus the laser beam to a spot of about 1 μm in diameter. The differential interference contrast (DIC) micrographs to exhibit the cell morphology were acquired in a transmission channel simultaneously. The three-dimensional (3D) distributions of TiO_2 nanoparticles and nuclei (or Golgi complexes) were obtained using the z-scan mode of the microscope.

Results and discussion

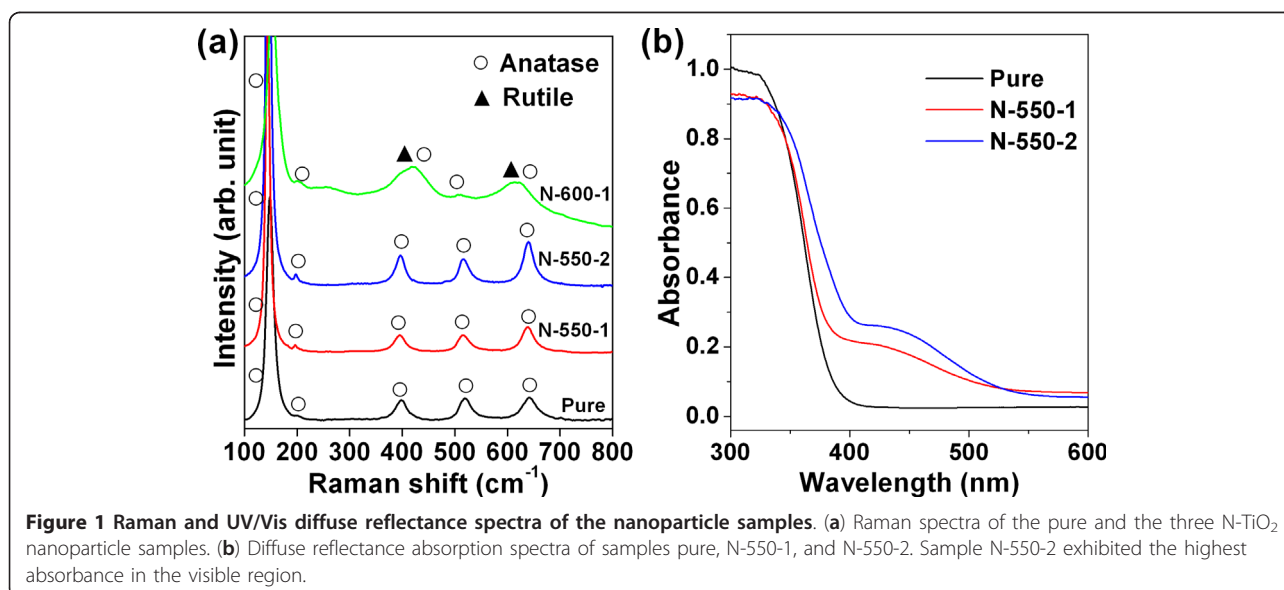### Raman spectra of TiO_2 nanoparticles

As shown in Table 1 and Figure 1a, the N-TiO_2 samples N-550-1 and N-550-2 with the calcination temperature of 550°C, as well as the pure TiO_2, exhibited a similar feature with five Raman peaks around 143, 197, 395, 514, and 640 cm^{-1}, corresponding to the Raman fundamental modes of the anatase phase [15,16]. The Raman peaks for rutile phase [16] around 238, 420, and 614 cm^{-1} appeared when the calcination temperature was 600°C as shown in the spectrum of the sample N-600-1. It can be concluded that the phase of the TiO_2 nanoparticles would transform from anatase to rutile when the calcination temperature increased to 600°C. Such a phase transformation will result in a decrease of the photocatalytic ability for TiO_2 powders [17,18]. Therefore, we only used samples N-550-1 and N-550-2 for further studies.

Absorption spectra of TiO_2 nanoparticles

Figure 1b shows the absorption spectra of the samples N-550-1 and N-550-2 and pure TiO_2. Compared to the pure TiO_2, the absorbances of N-550-1 and N-550-2 are higher in the visible region. However, the sample N-550-2 has the higher absorbance than N-550-1 in the region of 400 to 500 nm. Since N-550-1 and N-550-2 were calcinated at the same temperature and with the same amount of ammonia (flow rate times time), it seems that higher ammonia flow rate (N-550-2) could cause more absorption in the visible, which was expected to have higher photokilling efficiency of cells.

Cytotoxicity and photokilling effect

To evaluate the cytotoxicity of pure- and N-TiO_2 nanoparticles, the TiO_2-treated cells were further incubated in the dark for 28 h and the cell viability assays were then conducted. As shown in Figure 2a, all the surviving fractions of the treated HeLa cells were on the average values greater than 85% (with the concentration from 50 to 200 μg/mL). As shown in Figure 3, all the surviving fractions of the treated QGY or KB cells with the pure- or N-TiO_2 concentration of 200 μg/mL in the dark were greater than 85%. These results indicated that the cytotoxicities of pure- and N-TiO_2 nanoparticles were quite low. The cytotoxicities of these nanoparticles were quite similar, and there was no significant influence of the concentration on the cytotoxicity. Pure TiO_2 is biocompatible with primary and cancer cells [4]. Nitrogen is an essential element of many biological molecules, such as proteins and nucleic acids. So, nitrogen is not toxic if it does not exceed the normal levels. It could be understood that a small amount of nitrogen doping would not lead to more cytotoxicity than pure TiO_2.
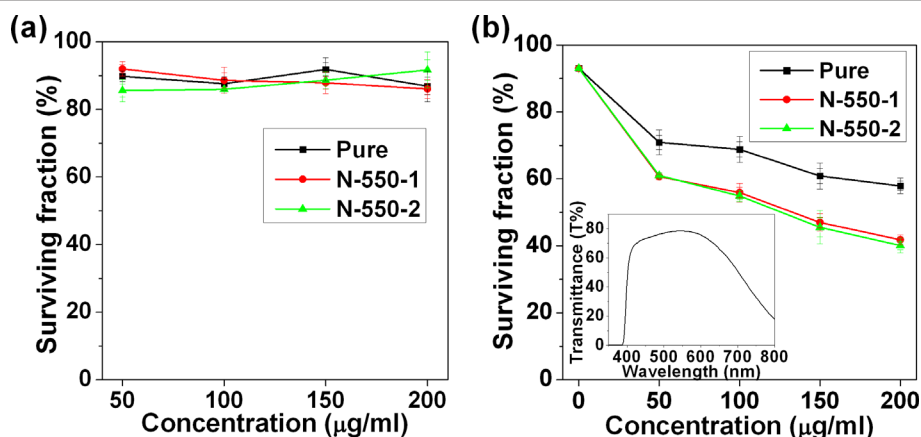

Figure 1 Raman and UV/Vis diffuse reflectance spectra of the nanoparticle samples. (**a**) Raman spectra of the pure and the three N-TiO_2 nanoparticle samples. (**b**) Diffuse reflectance absorption spectra of samples pure, N-550-1, and N-550-2. Sample N-550-2 exhibited the highest absorbance in the visible region.

Figure 2 Surviving fraction of treated and untreated HeLa cells. (a) Surviving fraction of HeLa cells as a function of the concentration of TiO_2 nanoparticles. HeLa cells were treated with 50, 100, 150, and 200 µg/mL TiO_2, respectively, in the dark. The surviving fraction of untreated cells (control group) was set as 100%. (b) The photokilling effects of pure and $N-TiO_2$ with different concentrations under visible irradiation. The inset is the transmittance spectrum of the combination of a 400 nm longpass filter and an IR cutoff filter used to acquire the visible-light irradiation from a Xe lamp.

The photokilling effects were measured as described in the experimental section. The surviving fractions of HeLa cells under visible-light irradiations for 4 h in dependence on the concentrations of pure- and $N-TiO_2$ nanoparticles were shown in Figure 2b. As demonstrated in Figure 2b, the visible light showed very little photokilling effect on HeLa cells in the absence of any TiO_2 (pure or N-doped) (at the 0 concentration). The surviving fractions (compared to the control cells without irradiation) were around 93%, which might be caused by the light irradiation, the fluctuant temperature during irradiation, and the experimental procedures. The spectrum of the light irradiated on cells (with filters) is also shown in the figure as an inset. It should be noted according to the spectrum in Figure 1b that the pure TiO_2 nanoparticles still has some absorption around 400 nm though the band gap of TiO_2 was reported to be 3.2 eV (corresponding to a wavelength of

387 nm). Therefore, pure TiO_2 exhibited some photokilling effect under visible-light irradiation as shown in Figure 2b. However, the cells treated with $N-TiO_2$ were killed more effectively than that with pure TiO_2. The photokilling effects of samples N-550-1 and N-550-2 were quite similar although their absorption spectra showed some difference. It is also demonstrated in Figure 2b that the survival fractions decreased with the increasing concentrations of the TiO_2 samples. It decreased to 40% for the cells treated with sample N-550-2 at a concentration of 200 µg/mL.

The photokilling effects of sample N-550-2 at a concentration of 200 µg/mL on QGY and KB cells were also measured as shown in Figure 3. Similar with the photokilling effect on HeLa cells, the QGY and KB cells treated with N-550-2 were also killed more effectively than that with pure TiO_2 under the visible-light irradiation. The results revealed that the $N-TiO_2$ might be applied to different cancers as a photosensitizer for PDT.
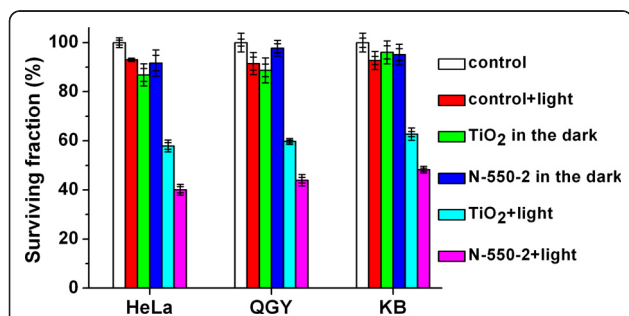
ROS influence on the photokilling effect

The mechanism of the photokilling effect for cancer cells caused by TiO_2 nanoparticles is very complex. It has been identified that UV-photoexcited TiO_2 in aqueous solution will result in formation of various ROS, such as hydroxyl radicals (·OH), hydrogen peroxide (H_2O_2), superoxide radicals (·O_2^-) and singlet oxygen ($^1O_2$) [19,20]. The ROS will attack the cancer cells and finally lead to the cell death. In order to study the function of ROS on the photokilling effect, the L-histidine, a quencher for both $^1O_2$ and ·OH [21-23], was added into the 96-well plates (20 mM) 30 min before the cells were

Figure 3 The cytotoxicities and the photokilling effects of pure TiO_2 and N-550-2 samples. With the concentration of 200 µg/mL on HeLa, QGY, and KB cells. The control groups were also shown for comparison.

irradiated by light. In the presence of 20 mM L-histidine, all the surviving fractions of the cells treated with pure- and N-TiO_2 at a concentration of 200 µg/mL increased evidently as shown in Figure 4. These results are similar to the previous report for UV-photoexcited TiO_2 [14]. It can be concluded that the ROS plays an important role on the photokilling effect, although we cannot tell which one played the main role. Further research is needed to figure out all the ROS influences.

Distribution of TiO_2 in cells

As is well-known, light-excited TiO_2 generates the electron-hole (e^-/h^+) pairs. The photogenerated carriers migrate to the particle surface and participate in various redox reactions there. Hence, the direct damage induced by photokilling effect would only occur at the sites of TiO_2 particles. Therefore, it is of importance to know if the TiO_2 nanoparticles were internalized into cells and how their intracellular distributions were. To find out the subcellular distribution of TiO_2 nanoparticles, the TiO_2-treated HeLa cells were stained with fluorescence indicators for Golgi complex and nucleus, respectively. Surprisingly, some TiO_2 nanoparticles were found inside the nuclei as shown in Figure 5, where the HeLa cells were treated with (N-550-2, 50 µg/mL) and stained with nuclear indicator. When these N-TiO_2-treated cells were irradiated by light from the Xe lamp with a 400-nm longpass filter (12 mW/cm^2) for 4 h, some micronuclei were observed as shown in Figure 6. Since the TiO_2 nanoparticles had entered into the nuclei of cells, the photoactivation effect could occur directly inside the nuclei, which might cause chromosomal damage or nucleus aberration. Micronuclei are usually formed from a chromosome or a fragment of a chromosome not incorporated into one of the daughter nuclei during cell
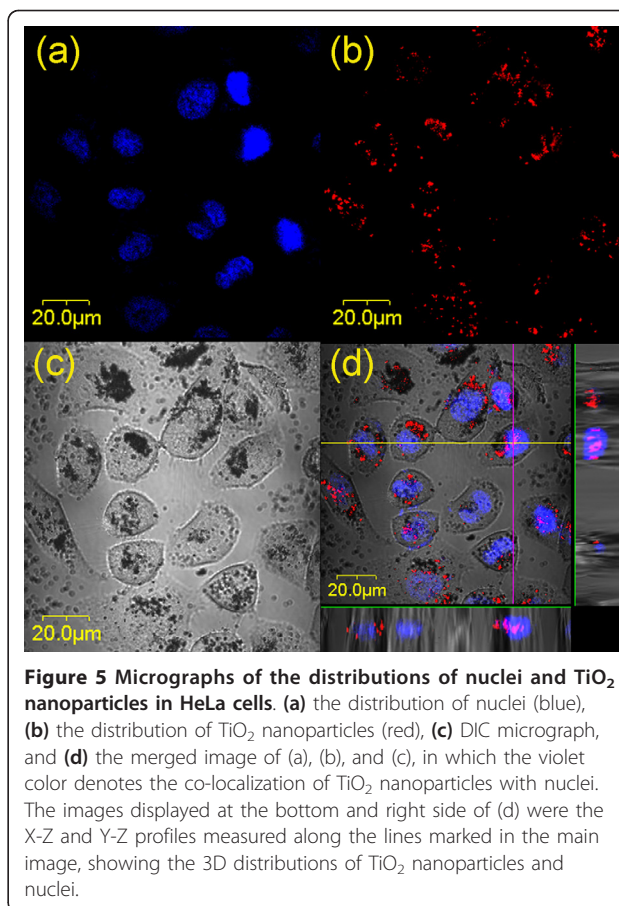

Figure 5 Micrographs of the distributions of nuclei and TiO_2 nanoparticles in HeLa cells. **(a)** the distribution of nuclei (blue), **(b)** the distribution of TiO_2 nanoparticles (red), **(c)** DIC micrograph, and **(d)** the merged image of (a), (b), and (c), in which the violet color denotes the co-localization of TiO_2 nanoparticles with nuclei. The images displayed at the bottom and right side of (d) were the X-Z and Y-Z profiles measured along the lines marked in the main image, showing the 3D distributions of TiO_2 nanoparticles and nuclei.
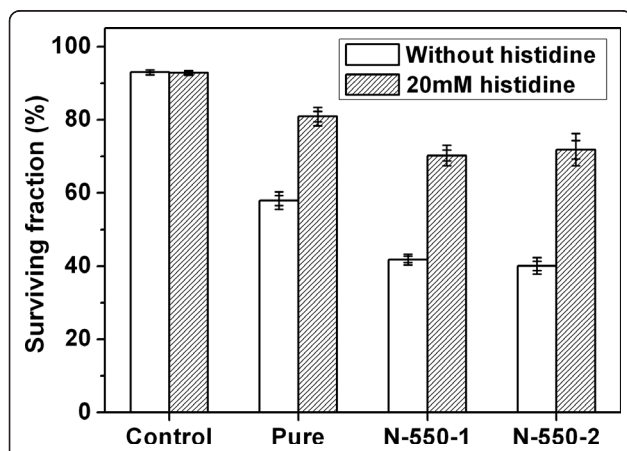

Figure 4 Changes in the surviving fractions of the TiO_2-treated HeLa cells with histidine. The concentration of the three TiO_2 samples is 200 µg/mL and L-histidine is 20 mM.
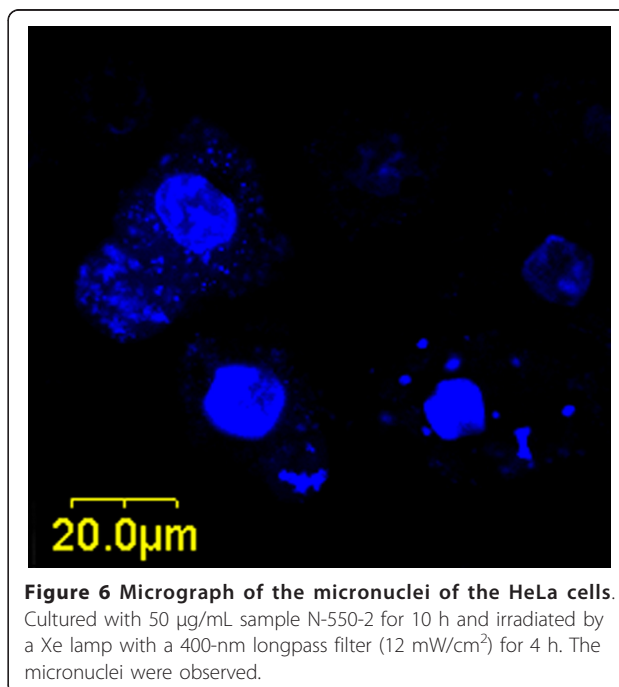

Figure 6 Micrograph of the micronuclei of the HeLa cells. Cultured with 50 µg/mL sample N-550-2 for 10 h and irradiated by a Xe lamp with a 400-nm longpass filter (12 mW/cm^2) for 4 h. The micronuclei were observed.

division. This is an evidence of the direct damage to the nucleus resulted from the photoexcited N-TiO$_2$ nanoparticles.

Figure 7 is the confocal micrographs to show the distributions of Golgi complexes (fluorescence image) and TiO$_2$ nanoparticles (reflection image) in HeLa cells. As shown in the merged image in Figure 7d, the TiO$_2$ particles were not only found on the cell membrane but also in the cytoplasm. Some TiO$_2$ nanoparticles aggregated around or in Golgi complexes. The co-localizations of TiO$_2$ with Golgi complexes (yellow color) were observed. The cell viability might be influenced by the localization of TiO$_2$ in Golgi complexes or other cell organelles, although there is no direct evidence found in this work.

Conclusions

In the present work, N-TiO$_2$ nanoparticles were prepared by calcination under ammonia atmosphere, which is an easily operative method and can achieve the product fruitfully. All the cytotoxicities of the pure- or N-TiO$_2$ nanoparticles were quite low. The N-TiO$_2$ samples showed higher absorbance and better photokilling effect than the pure TiO$_2$ in the visible region. Therefore, the N-TiO$_2$ has a higher potential as a photosensitizer for PDT of cancers.

TiO$_2$ is nonfluorescent and cannot be detected by fluorescence imaging. However, it can be monitored by the reflection imaging, which makes it convenient to record simultaneously with the fluorescence image using a LSCM. Co-localization of N-TiO$_2$ nanoparticles with nuclei was observed. After visible-light irradiation, some micronuclei were detected as a sign of the nucleus aberration. Furthermore, ROS was found to play an important role on the photokilling effect for cells. However, the mechanisms for the photokilling effect on cancer cells should be investigated in details further.

Author details

[1]Key Laboratory of Micro and Nano Photonic Structures (Ministry of Education), Department of Optical Science and Engineering, Fudan University, Shanghai 200433, China [2]Surface Physics Laboratory (National Key Laboratory), Department of Physics, Fudan University, Shanghai 200433, China

Authors' contributions

ZL carried out the experiments and drafted the manuscript. LM designed the project, participated in the confocal microscopy imaging, and wrote the manuscript. PW supervised the work and participated in the discussion of the results and in revising the manuscript. JC participated in the discussion of the results. All authors read and approved the final manuscript.

Competing interests

The authors declare that they have no competing interests.

Figure 7 Micrographs of the distributions of Golgi complexes and TiO$_2$ nanoparticles in HeLa cells. **(a)** The distribution of Golgi complexes (green), **(b)** the distribution of TiO$_2$ nanoparticles (red), **(c)** differential interference contrast (DIC) micrograph, and **(d)** the merged image of (a), (b), and (c), in which the yellow color denotes the co-localization of TiO$_2$ nanoparticles with Golgi bodies. The images displayed at the bottom and right side of (d) were the X-Z and Y-Z profiles measured along the lines marked in the main image, showing the 3D distributions of TiO$_2$ and Golgi bodies.

References

1. Szacilowski K, Macyk W, Drzewiecka-Matuszek A, Brindell M, Stochel G: **Bioinorganic photochemistry: Frontiers and mechanisms.** *Chem Rev* 2005, **105**:2647-2694.
2. Warheit DB, Hoke RA, Finlay C, Donner EM, Reed KL, Sayes CM: **Development of a base set of toxicity tests using ultrafine TiO$_2$ particles as a component of nanoparticle risk management.** *Toxicol Lett* 2007, **171**:99-110.
3. Fabian E, Landsiedel R, Ma-Hock L, Wiench K, Wohlleben W, van Ravenzwaay B: **Tissue distribution and toxicity of intravenously administered titanium dioxide nanoparticles in rats.** *Arch Toxicol* 2008, **82**:151-157.
4. Carbone R, Marangi I, Zanardi A, Giorgetti L, Chierici E, Berlanda G, Podestà A, Fiorentini F, Bongiorno G, Piseri P, Pelicci PG, Milani P: **Biocompatibility of cluster-assembled nanostructured TiO$_2$ with primary and cancer cells.** *Biomaterials* 2006, **27**:3221-3229.
5. Adams LK, Lyon DY, Alvarez PJ: **Comparative eco-toxicity of nanoscale TiO$_2$, SiO$_2$, and ZnO water suspensions.** *Water Res* 2006, **40**:3527-3532.
6. Thevenot P, Cho J, Wavhal D, Timmons RB, Tang LP: **Surface chemistry influences cancer killing effect of TiO$_2$ nanoparticles.** *Nanomed-Nanotechnol* 2008, **4**:226-236.
7. Brunet L, Lyon DY, Hotze EM, Alvarez PJJ, Wiesner MR: **Comparative photoactivity and antibacterial properties of C$_{60}$ fullerenes and titanium dioxide nanoparticles.** *Environ Sci Technol* 2009, **43**:4355-4360.
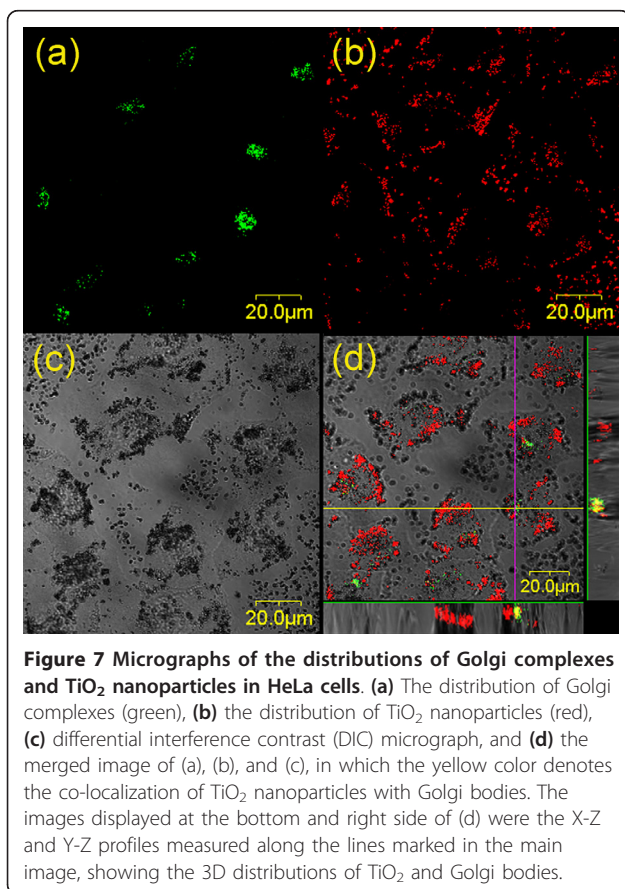
8. Choi O, Hu ZQ: Role of reactive oxygen species in determining nitrification inhibition by metallic/oxide nanoparticles. *J Environ Eng-Asce* 2009, **135**:1365-1370.
9. Lagopati N, Kitsiou PV, Kontos AI, Venieratos P, Kotsopoulou E, Kontos AG, Dionysiou DD, Pispas S, Tsilibary EC, Falaras P: Photo-induced treatment of breast epithelial cancer cells using nanostructured titanium dioxide solution. *J Photoch Photobio A* 2010, **214**:215-223.
10. Zhang DQ, Li GS, Yu JC: Inorganic materials for photocatalytic water disinfection. *J Mater Chem* 2010, **20**:4529-4536.
11. Xu SJ, Shen JQ, Chen S, Zhang MH, Shen T: Active oxygen species ($^1O_2$, O_2^{-}) generation in the system of TiO_2 colloid sensitized by hypocrellin B. *J Photoch Photobio B* 2002, **67**:64-70.
12. Tokuoka Y, Yamada M, Kawashima N, Miyasaka T: Anticancer effect of dye-sensitized TiO_2 nanocrystals by polychromatic visible light irradiation. *Chem Lett* 2006, **35**:496-497.
13. Janczyk A, Wolnicka-Głubisz A, Urbanska K, Stochel G, Macyk W: Photocytotoxicity of platinum(IV)-chloride surface modified TiO_2 irradiated with visible light against murine macrophages. *J Photoch Photobio B* 2008, **92**:54-58.
14. Janczyk A, Wolnicka-Głubisz A, Urbanska K, Kisch H, Stochel G, Macyk W: Photodynamic activity of platinum(IV) chloride surface-modified TiO_2 irradiated with visible light. *Free Radical Bio Med* 2008, **44**:1120-1130.
15. Chen XB, Lou YB, Samia ACS, Burda C, Gole JL: Formation of oxynitride as the photocatalytic enhancing site in nitrogen-doped titania nanocatalysts: Comparison to a commercial nanopowder. *Adv Funct Mater* 2005, **15**:41-49.
16. Wang H, Wu Y, Xu BQ: Preparation and characterization of nanosized anatase TiO_2 cuboids for photocatalysis. *Appl Catal B* 2005, **59**:139-146.
17. Mi L, Xu P, Wang PN: Experimental study on the bandgap narrowings of TiO_2 films calcined under N_2 or NH_3 atmosphere. *Appl Surf Sci* 2008, **255**:2574-2580.
18. Wantala K, Laokiat L, Khemthong P, Grisdanurak N, Fukaya K: Calcination temperature effect on solvothermal Fe-TiO_2 and its performance under visible light irradiation. *J Taiwan Inst Chem E* 2010, **41**:612-616.
19. Daimon T, Nosaka Y: Formation and behavior of singlet molecular oxygen in TiO_2 photocatalysis studied by detection of near-infrared phosphorescence. *J Phys Chem C* 2007, **111**:4420-4424.
20. Tachikawa T, Majima T: Single-molecule detection of reactive oxygen species: application to photocatalytic reactions. *J Fluoresc* 2007, **17**:727-738.
21. Wade AM, Tucker HN: Antioxidant characteristics of L-histidine. *J Nutr Biochem* 1998, **9**:308-315.
22. Schweitzer C, Schmidt R: Physical mechanisms of generation and deactivation of singlet oxygen. *Chem Rev* 2003, **103**:1685-1757.
23. Redmond RW, Kochevar IE: Spatially resolved cellular responses to singlet oxygen. *Photochem Photobiol* 2006, **82**:1178-1186.